Inorganic Chemistry

Article

pubs.acs.org/IC

Effect of Structural Isomerism on Magnetic Dynamics: from Single-Molecule Magnet to Single-Chain Magnet

Ting-Ting Wang,[†] Min Ren,[†] Song-Song Bao,[†] Bin Liu,[‡] Li Pi,[§] Zhong-Sheng Cai,[†] Ze-Hua Zheng,[†] Zhong-Li Xu,[†] and Li-Min Zheng*,[†]

[†]School of Chemistry and Chemical Engineering, State Key Laboratory of Coordination Chemistry, Nanjing University, Nanjing 210093, P. R. China

[‡]Key Laboratory of Synthetic and Natural Functional Molecule Chemistry of the Ministry of Education, Shaanxi Key Laboratory of Physico-Inorganic Chemistry, College of Chemistry & Materials Science, Northwest University, Xi'an 710069, P. R. China

[§]High Magnetic Field Laboratory, Chinese Academy of Sciences, Hefei 230031, P. R. China

Supporting Information

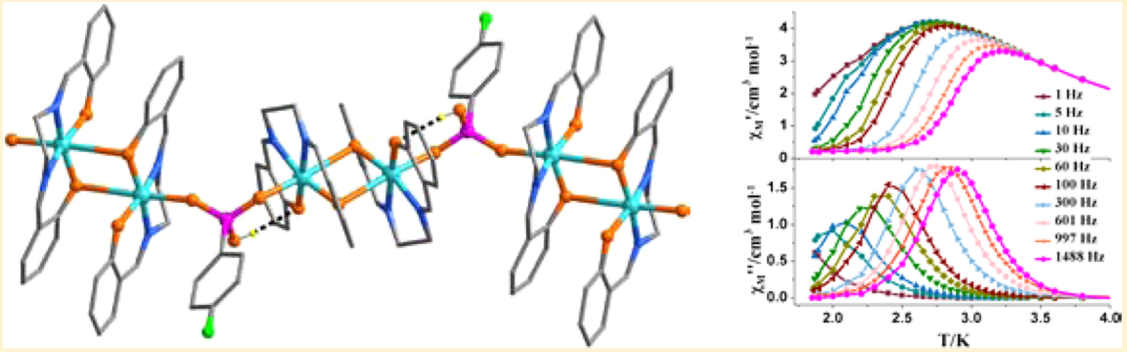

ABSTRACT: This Paper reports the first examples of O−P−O bridged $Mn_2(salen)_2$ (salen = *N*,*N*′-bis(salicylidene)-ethylenediamine) chain compounds, namely, $[Mn_2(salen)_2(2\text{-}FC_6H_4PO_3H)](ClO_4)\cdot 1/2CH_3OH$ (**1**) and $[Mn_2(salen)_2(4\text{-}FC_6H_4PO_3H)](ClO_4)$ (**2**). The phosphonate ligands adopt a *syn-anti* bidentate bridging mode in **1** and a *syn-syn* bidentate bridging mode in **2**, originated from the isomeric phosphonate ligands. The different bridging modes cause a significant change in the Mn−O···O−Mn torsion angle over the O−P−O bridge, which are 96.6 and 1.9° for **1** and **2**, respectively. As a result, the antiferromagnetic (AF) exchange couplings mediated through the O−P−O pathway are extremely weak in **1**, and the overall magnetic behaviors are dominated by the $Mn_2(salen)_2$ moieties. Single-molecule magnetic behavior is observed in **1**. For compound **2**, the AF interaction over the O−P−O bridge is much stronger. The coexistence of metamagnetism and single-chain magnetic behavior is observed for **2**.

INTRODUCTION

Since the discovery of the first single-chain magnet (SCM) in a magnetically isolated $Co^{II}(hfac)_2$/radical (hfac = hexafluoroacetylacetone) compound,[1] molecular chain systems showing slow magnetization relaxation have received great attention due to their potential applications in information storage and molecular spintronics.[2,3] A number of SCMs have been reported, some of which exhibit the coexistence of SCM behavior and antiferromagnetism or metamagnetism.[4−6] Several strategies have been proposed to obtain SCMs, among which one efficient approach is to organize specific single-molecule magnet (SMM) building blocks into chain structures.[7] However, the interpretation of the magnetic properties of such systems is complicated, because even weak inter-SMM interaction can perturb the intrinsic SMM properties.[8,9] If the inter-SMM interaction is strong enough, SCMs or even long-range ordering magnets can be obtained. To achieve SCMs based on SMM building blocks, it is essential to modulate the inter-SMM interactions within the chain and between the chains. Today, there are few examples of SCMs based on SMM building units, such as the Mn^{III} Schiff base (SB) out-of-plane dimers $[Mn_2(SB)_2]$,[10−14] Mn_3O,[15] $Mn_4(hmp)_6$,[16] and other Mn_x clusters.[17] The manipulation of the magnetic dynamics of these chain systems remains a great challenge.

Phosphonates, as an important class of three-atom bridges, have been used to construct a variety of complexes with unique network topologies and interesting physical or chemical properties.[18] Metal phosphonates are also promising in molecular magnetism as SMMs,[19] SCMs,[20] long-range ordering,[21] and tunable magnetic materials.[22] Since the O−P−O bridge is quite flexible when coordinating with metal ion, the nature of the exchange couplings through O−P−O bridge is

Received: December 10, 2013
Published: March 4, 2014

   dx.doi.org/10.1021/ic403042p | Inorg. Chem. 2014, 53, 3117−3125

not very clear. In a recent study on the isomeric copper phosphonates, we found that the metal···metal distances and metal-O···O-metal torsion angles over the O−P−O bridge should play a key role in determining the nature and magnitude of the magnetic exchange couplings.[23] The flexibility of the phosphonate bridge also offers a unique opportunity to modulate the magnetic behaviors of such systems through structural modification.

In this Paper, we present the first examples of the phosphonate-bridged $Mn_2(SB)_2$ chain compounds, namely, $[Mn_2(salen)_2(2\text{-}FC_6H_4PO_3H)](ClO_4)\cdot 1/2CH_3OH$ (**1**) and $[Mn_2(salen)_2(4\text{-}FC_6H_4PO_3H)](ClO_4)$ (**2**) (salen = *N*,*N*′-bis(salicylidene)ethylenediamine) (Scheme 1). Compound **1** shows SMM behavior, while compound **2** displays the coexistence of SCM and metamagnetism. The results demonstrate that the magnetic dynamics of the phosphonate-bridged $Mn_2(SB)_2$ chain may be modulated by using positional isomeric bridging ligands. To the best of our knowledge, only two examples of SCMs have been reported where the magnetic centers are linked by O−P−O units, including $[Mn(TPP)\text{-}O_2PHPh]\cdot H_2O$ (TPP = *meso*-tetraphenylporphyrin)[24] and $[Co(H_2L^1)(H_2O)]$ (L^1 = 4-Me−C_6H_4−$CH_2(CPO_3H_2)_2$).[20]

Scheme 1. Formation of Compounds 1 and 2

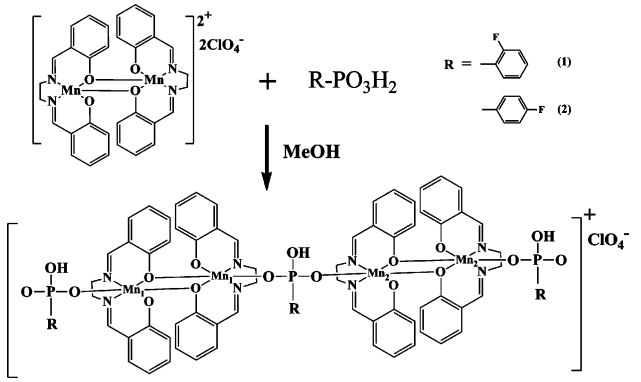

EXPERIMENTAL SECTION

Starting Materials. All experiments were performed in air. Salicylaldehyde, 1,2-ethanediamine, manganese acetate dihydrate, and sodium perchlorate monohydrate were purchased from commercial sources and used as received. All solvents were reagent grade and used without further purification. $[Mn(salen)(H_2O)]_2(ClO_4)_2$ was prepared according to the modified literature procedure.[25] The 2-fluorophenylphosphonic acid[26] and 4-fluorophenylphosphonic acid[26] were prepared according to the literature.

Caution! Perchlorate salts are potentially explosive and should be handled carefully.

Synthesis of Compound 1. A methanol solution (10 cm^3) of 2-fluorophenylphosphonic acid (0.0176 g, 0.1 mmol) was added to a methanol solution (10 cm^3) of the $[Mn(salen)(H_2O)]_2(ClO_4)_2$ (0.0877 g, 0.1 mmol) compound. The solution was stirred for 12 h and left in air for one week. Dark brown block-like crystals of compound **1** were collected, with a yield of 55%. Elemental analysis calcd. for $C_{77}H_{70}Cl_2F_2Mn_4N_8O_{23}P_2$: C, 49.56; H, 3.78; N, 6.00. Found: C, 49.63; H, 3.74; N, 6.00%. IR (KBr, cm^{-1}): 3406(w), 1625(s), 1601(s), 1544(s), 1472(w), 1446(s), 1390(w), 1332(w), 1297(s), 1204(w), 1177(w), 1149(w), 1132(m), 1097(s), 933(w), 905(m), 803(m), 751(s), 623(m), 596(m), 461(m).

Synthesis of Compound 2. Compound **2** was prepared as dark-brown block-like crystals, following the same procedure as that for **1**, but the 2-fluorophenylphosphonic acid was replaced by 4-fluorophenylphosphonic acid. Yield: 71%. Elemental analysis calcd. for $C_{76}H_{66}Cl_2F_2Mn_4N_8O_{22}P_2$: C, 49.77; H, 3.63; N, 6.11. Found: C, 50.86; H, 3.66; N, 6.26%. IR (KBr, cm^{-1}): 3407(w), 1622(s), 1560(s), 1542(s), 1504(w), 1469(m), 1446(s), 1390(w), 1338(w), 1295(s), 1203(m), 1181(m), 1152(s), 1131(m), 1096(s),1050(m), 973(w), 929(w), 905(m), 874(s), 834(w), 802(m), 763(s), 754(s), 624(m), 591(m), 539(m), 461(m).

Physical Measurements. Elemental analyses for C, H, and N were performed at the Perkin-Elmer 240C elemental analyzer. Infrared (IR) spectra were measured as KBr pellets on a VECTOR 22 spectrometer in the range of 400−4000 cm^{-1}. Powder X-ray diffraction (PXRD) data were recorded on a Bruker D8 ADVANCE X-ray powder diffractometer (Cu Kα) over the 2θ range of 5 to 40° at room temperature. Thermogravimetric analyses were performed with a Mettler-Toledo TGA/DSC STARe thermal analyzer in the range of 25−800 °C under a nitrogen flow at a heating rate of 5 °C min^{-1}. The magnetic susceptibility data were performed on a Quantum Design MPMS-XL7 SQUID magnetometer. Using Pascal's constants, the data

Table 1. Crystallographic Data for Compounds 1 and 2

	1	2
empirical formula	$C_{77}H_{70}Cl_2F_2Mn_4N_8O_{23}P_2$	$C_{76}H_{66}Cl_2F_2Mn_4N_8O_{22}P_2$
Fw	1866.01	1833.97
crystal system	triclinic	triclinic
space group	$P\bar{1}$	$P\bar{1}$
a (Å)	10.8532(15)	10.314(4)
b (Å)	13.2141(18)	13.464(6)
c (Å)	14.515(2)	14.790(6)
α (deg)	69.045(2)	99.551(6)
β (deg)	79.784(2)	110.280(5)
γ (deg)	88.200(2)	100.085(6)
V (Å^3), Z	1912.0(5), 1	1838.8(13), 1
Dc (g·cm^{-3})	1.621	1.656
μ (mm^{-1})	0.847	0.878
F (000)	954	936
$R_1{}^a$, $wR_2{}^b$ [$I > 2\sigma(I)$]	0.0451, 0.1249	0.0666, 0.1068
$R_1{}^a$, $wR_2{}^b$ (all data)	0.0572, 0.1351	0.1754, 0.1322
goodness-of-fit	1.115	0.850
$(\Delta\rho)_{max}$, $(\Delta\rho)_{min}$ (e Å^{-3}) CCDC	1.037, −0.752 936456	0.546, −0.376 936457

$^aR_1 = \Sigma||F_o| - |F_c||/\Sigma|F_o|$. $^bwR_2 = [\Sigma w(F_o^2 - F_c^2)^2/\Sigma w(F_o^2)^2]^{1/2}$

dx.doi.org/10.1021/ic403042p | Inorg. Chem. 2014, 53, 3117−3125

were corrected for diamagnetic contributions of both the sample holder and the compound obtained.[27]

Single Crystal Structure Determination. Single crystals of dimensions 0.14 × 0.12 × 0.03 mm^3 for **1** and 0.22 × 0.16 × 0.09 mm^3 for **2** were mounted on a glass rod. The crystal data were collected with a Bruker SMART CCD diffractometer using monochromated Mo Kα radiation (λ = 0.71073 Å) at 163 K. A hemisphere of data was collected in the θ range of 1.53−25.00° for **1** and 1.58−26.00° for **2**, using a narrow-frame method with scan widths of 0.30° in ω and an exposure time of 5 s/frame. The numbers of observed and unique reflections are 13 848 and 6675 (R_{int} = 0.0291) for **1**, and 14 473 and 7138 (R_{int} = 0.1191) for **2**. The data were integrated using the Siemens *SAINT* program,[28] with the intensities corrected for Lorentz factor, polarization, air absorption, and absorption due to variation in the path length through the detector faceplate. Multiscan absorption corrections were applied. The structures were solved by direct methods and refined on F^2 by full-matrix least-squares using *SHELXTL*.[29] All the non-hydrogen atoms were located from the Fourier maps and were refined anisotropically. All H atoms were refined isotropically, with the isotropic vibration parameters related to the non-H atom to which they are bonded. The crystallographic data for compounds **1** and **2** are provided in Table 1. Selected bond lengths and angles for compounds **1** and **2** are given in Supporting Information, Tables S1−S2.

RESULTS AND DISCUSSION

Crystal Structures. Compound **1** crystallizes in triclinic space group $P\bar{1}$. The asymmetric unit contains two $Mn(salen)^+$, one 2-$FC_6H_4PO_3H^-$, one ClO_4^-, and 0.5 CH_3OH. Each Mn atom has a distorted octahedral geometry with the four equatorial positions occupied by two O and two N atoms from the salen ligand [Mn−O(N): 1.873(2)−1.998(3) Å] and two axial positions by the phosphonate oxygen atoms [Mn−O(P): 2.096(2)−2.815(2) Å] (Figure 1a). The phenoxo atoms O2 and O3 behave as μ_3-O, linking the equivalent Mn(salen) units into a dimer. The Mn1···Mn1 and Mn2···Mn2 distances over the phenoxo bridges are 3.488(1) and 3.537(1) Å, respectively. The Mn−O−Mn angles are 95.6(1)−98.4(1)°. The 2-fluorophenylphosphonate adopts a *syn-anti* coordination mode (Scheme 2) and cross-links the $Mn1_2O_2$ and $Mn2_2O_2$ dimers into a chain (Figure 1b). The Mn1···Mn2 distance over the O−P−O bridge is 5.578(1) Å. The Mn1−O···O−Mn2 torsion angle is 96.6°. Moderate strong hydrogen bonds are found between neighboring chain [O7···O6C: 2.683(3) Å], forming a supramolecular layer in the *ac* plane (Figure 1c). The ClO_4^- anion and CH_3OH molecules reside between the layers with hydrogen bond interactions within or between the layers (Supporting Information, Figures S4 and S5). The shortest Mn···Mn distance between the chains is 7.152(1) Å.

Compound **2** crystallizes in triclinic space group $P\bar{1}$. It also shows a zigzag chain structure in which the $Mn1_2O_2$ and $Mn2_2O_2$ dimers are alternatively linked by the phosphonate ligands (Figure 2). The Mn−O(P) bond lengths are in the range of 2.085(4)−2.501(4) Å. Within the chain, the Mn1···Mn1, Mn2···Mn2, and Mn1···Mn2 distances are 3.544(2), 3.340(2), and 6.024(2) Å, respectively. The Mn−O−Mn angles are 97.5(1)−98.2(2)°. One significant feature of structure **2** is that the 4-fluorophenylphosphonate ligand adopts a *syn-syn* coordination mode (Scheme 2). This poses remarkable influences on the structure. The Mn1−O···O−Mn2 torsion angle is reduced significantly to 1.9°. The protonated phosphonate oxygen (O7) forms hydrogen bonds within the chain [O7···O1: 2.945(4) Å] (Figure 2b), instead of between the chains as in compound **1**. Although weak C−H···O hydrogen bond interactions are observed between the salen ligands and perchlorate groups (Supporting Information, Figure S6), the shortest interchain Mn···Mn distance is significantly enlarged in **2** [9.148(2) Å vs 7.152(1) Å in **1**].

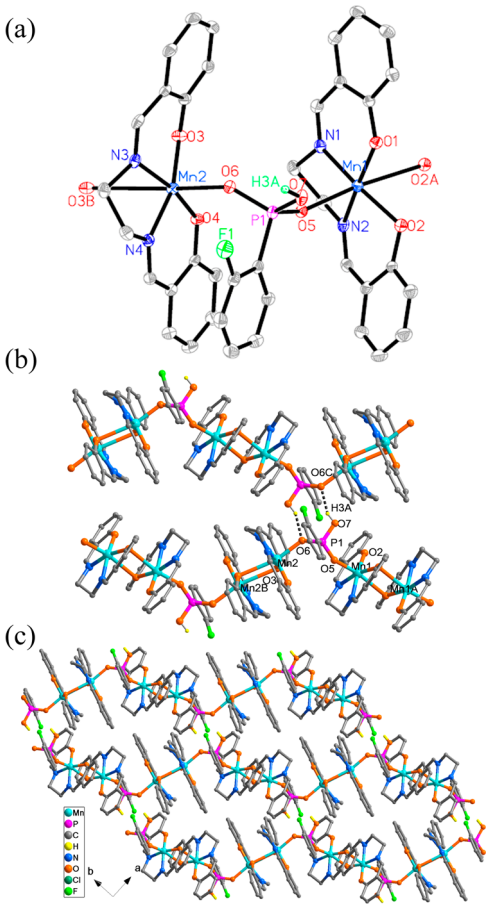

Figure 1. (a) Building unit of **1** showing the atomic numbering scheme (30% probability). (b) The adjacent chains in **1** with interchain hydrogen bond interactions. Symmetry code: C: 1 − *x*, 2 − *y*, −*z*. (c) Two-dimensional supramolecular layer in the *ab* plane in **1**.

Scheme 2. The Coordination Modes of the Phosphonate Ligands

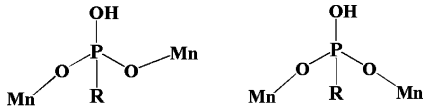

syn-anti mode *syn-syn* mode

Considering that compounds **1** and **2** were prepared under similar reaction conditions, the adoption by the phosphonate ligand of a *syn-anti* mode in **1** and a *syn-syn* mode in **2** must be related to the positional isomeric phosphonate ligands. In **1**, the $Mn_2(salen)_2$ dimers are linked by 2-fluorophenylphosphonate. The C−H···F interaction is found between the salen and phosphonate ligands within the chain [C···F: 3.399(4) Å, C−H···F: 153.6(2)°] (Figure 3a).[30a] In **2**, however, 4-fluorophenylphosphonate serves as the linkage, and the C−H···F interaction [C···F: 3.246(8) Å, C−H···F: 126.4(4)°] is observed between the chains (Figure 2b). A careful analysis reveals that the rigid phenyl ring of 4-fluorophenylphosphonate shifts slightly to form C−H···π bonds with the neighboring phenyl groups of salen (Figure 3b).[30b] Such weak interactions

dx.doi.org/10.1021/ic403042p | *Inorg. Chem.* 2014, 53, 3117−3125

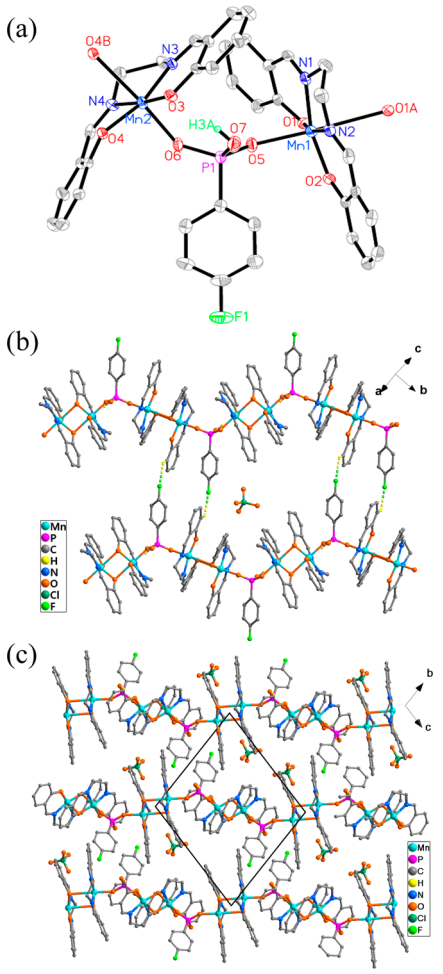

Figure 2. (a) Building unit of **2** showing the atomic numbering scheme (30% probability). (b) The adjacent chains in **2** with C−H···F interactions between the chains. (c) The packing diagram of **2** viewed along the *a* axis. All the hydrogen atoms have been omitted for clarity.

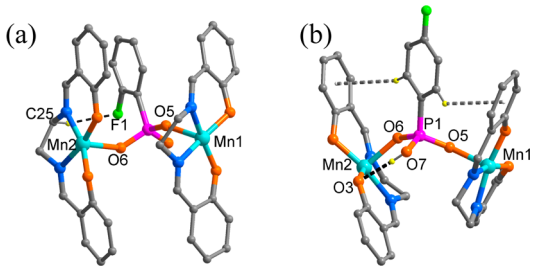

Figure 3. Weak interactions between the phosphonate and salen ligands within the chain in compounds **1** (a) and **2** (b).

cause a slight difference in the arrangement of the Mn(salen) planes across the O−P−O bridges. If we define each Mn(salen) plane by its two N and two O atoms, the dihedral angles of Mn(salen) planes across the O−P−O bridges (β) are 71.0° for **1** and 63.4° for **2**. Apparently, it must be the weak intrachain interactions between the phosphonate and the salen ligands that determines the particular coordination mode of the phosphonate ligand and hence the intra- and interchain structures. The structural difference will be reflected by their magnetic properties.

Magnetic Properties of 1. The static magnetic susceptibilities were measured under 2 kOe (for **1**) or 1 kOe (for **2**) direct current (dc) fields. At 300 K, the $\chi_M T$ values per Mn^{III}_2 unit are 5.94 and 6.36 $cm^3 \cdot K \cdot mol^{-1}$ for **1** and **2**, respectively, close to the theoretical value of 6.00 $cm^3 \cdot K \cdot mol^{-1}$ expected for two spins with $S = 2$ and $g = 2$.

For compound **1**, the $\chi_M T$ value increases gradually upon cooling from room temperature and then increases sharply, reaching a maximum of 8.01 $cm^3 \cdot K \cdot mol^{-1}$ at 7.00 K, indicating a dominant ferromagnetic interaction between the Mn^{III} centers (Figure 4). Below the cusp temperature, the $\chi_M T$ value

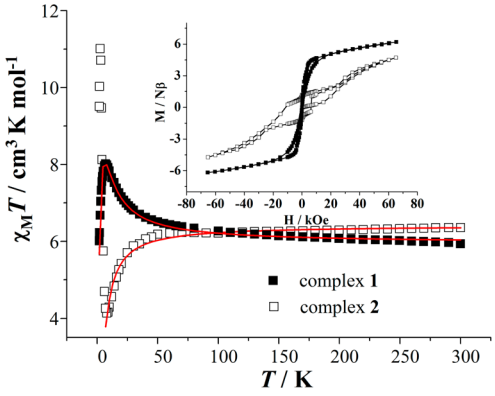

Figure 4. Plots of the $\chi_M T$ vs T for **1** and **2**. The solid lines represent the best fit of the data according to the alternating chain model. (inset) The M vs H plots for **1** and **2** at 0.5 K.

experiences a sudden decrease to 6.01 $cm^3 \cdot K \cdot mol^{-1}$ at 1.8 K, attributed to the interchain antiferromagnetic exchange and/or the zero-field splitting of the ground state. The magnetic susceptibility above 100 K obeys the Curie−Weiss law with C = 5.81 $cm^3 \cdot K \cdot mol^{-1}$ and θ = 8.07 K (Supporting Information, Figure S7). The positive θ value ascertains a dominant ferromagnetic coupling in **1**.

There are two different magnetic exchange pathways in compound **1**. One is through the phenolate bridge ($2J_1$), and the other is through the O−P−O bridge ($2J_2$) (Scheme 3).

Scheme 3. Schematic View of Exchange Pathways in Complexes 1 and 2

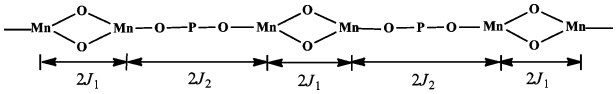

Considering that the Mn−O···O−Mn torsion angle in **1** is quite large [96.6° (or 83.4°)], the antiferromagnetic (AF) interaction through the O−P−O bridge could be very weak.[23] The overall ferromagnetic exchange coupling should mainly arise from the phenolate oxygen pathway within the $[Mn_2(salen)_2]^{2+}$ dimer. Assuming that the exchange couplings within the $Mn1_2O_2$ and $Mn2_2O_2$ dimers are the same ($2J_1$), the magnetic susceptibilities of **1** can be simulated by using a dimer model based on Hamiltonian $H = -2J_1 S_{Mn} S_{Mn} + g_{Mn}\beta(S_{Mn} + S_{Mn}) \cdot H$.[27] The best fit results in parameters g = 1.99, J_1 = 0.79 K, zJ' = −0.02 K, and $R = 2.30 \times 10^{-3}$, where zJ' accounts for the interdimer interactions over the O−P−O bridge in the mean field approximation. The susceptibility data can also be simulated with the alternating chain model by Rojo formula (for $S = 2$), the nearest neighbor exchange interactions described by the spin Hamiltonian $H = -2J_1 \Sigma S_{2i} S_{2i+1} + -2J_2 \Sigma S_{2i+1} S_{2i+2}$.[31] The best fit, shown as the solid line in Figure 4,

dx.doi.org/10.1021/ic403042p | Inorg. Chem. 2014, 53, 3117−3125

results in parameters $g = 1.99$, $J_1 = 2.58$ K, $J_2 = -0.33$ K, and $R = 7.90 \times 10^{-3}$. The positive J_1 value is comparable to those in the other $[Mn_2(SB)_2]^{2+}$ dimers.[32]

To study the magnetic dynamics of compound **1**, the temperature-dependent alternating current (ac) susceptibilities were measured under zero dc field in the frequency range of 884−1488 Hz with an oscillating 3 Oe ac field. As shown in Supporting Information, Figure S8, both the χ_M' and χ_M'' signals are frequency-dependent below 4.0 K, indicating a slow relaxation of magnetization characteristic of an SMM or SCM. But the maximum of χ_M'' is only clearly observed above 1116 Hz, making it impossible to derive the energy barrier of the magnetization reversal. It is well-known that the magnetization relaxation of SMMs could be affected by the quantum tunneling of magnetization (QTM).[33] The QTM effect can be suppressed by applying an external dc field. To investigate the effect of the static field on the magnetization relaxation of compound **1**, ac measurements were performed at 1.8 K with various applied dc fields (Supporting Information, Figure S9). The magnetization relaxation time τ can be extracted by fitting the Cole−Cole plots using the generalized Debye model (Supporting Information, Figure S10).[34,35] As shown in Supporting Information, Figure S11, the application of dc field slows down the relaxation process. The relaxation time increases from 0.23 ms (zero field) to 6.95 ms (2.5 kOe). However, the α value increases dramatically from 0.178 (zero field) to 0.633 (2.5 kOe), suggesting that the relaxation process under high field could deviate from a typical SMM. Thus the temperature-dependent ac susceptibilities were measured under 1 kOe dc field. Peaks of χ_M'' appear in the χ_M'' versus T curves in the frequency range of 884−1488 Hz (Supporting Information, Figure S12). The relaxation time follows the Arrhenius law $\tau = \tau_0 \exp(\Delta/k_BT)$, where Δ/k_B is the effective energy barrier for the reversal of the magnetization, τ_0 is the pre-exponential factor, and k_B is the Boltzmann constant. The resulting values of Δ/k_B and τ_0 are 18.6 K and 5.0×10^{-8} s, respectively (Supporting Information, Figure S13).

The variable-frequency ac magnetic susceptibility measurements were also conducted under zero and 1 kOe dc fields in the temperature range of 1.8−3.3 K (Figure 5). The decline in the χ_M' component is accompanied with the appearance of peaks in the χ_M'' component, indicating slow relaxation of magnetization. The magnetization relaxation time τ can be extracted by fitting the Cole−Cole plots using the generalized Debye model (Figure 5c,d). A linear dependence is found in the lnτ versus $1/T$ plot. The Δ/k_B and τ_0 values deduced from the Arrhenius laws are 13.5 K and 1.4×10^{-7} s under zero dc field and 19.7 K and 2.5×10^{-8} s under 1 kOe dc field, respectively (Figure 6). The energy barriers are comparable to those found for the other SMMs based on $Mn^{III}_2(SB)_2$ dimers.[7b,8] The τ_0 values are typical for SMMs (10^{-7}−10^{-8} s),[36] suggesting that compound **1** is an SMM.

The increase of the energy barrier under 1 kOe dc field, compared with that in zero dc field, can be due to the suppression of the QTM effect. The distribution coefficient α values under zero and 1 kOe dc fields are within the range of 0.05−0.19 (1.82−2.60 K) and 0.07−0.21 (1.90−3.30 K), respectively, indicating a narrow distribution of the relaxation. Since the energy barrier Δ/k_B for an SMM is equal to $|D|S_T^2/k_B$, the uniaxial anisotropy for the dimer ($S_T = 4$) can be deduced as $D_{Mn2}/k_B = -1.23$ K. This value is in agreement with those obtained for the other $Mn_2(SB)_2$ dimers.[32]

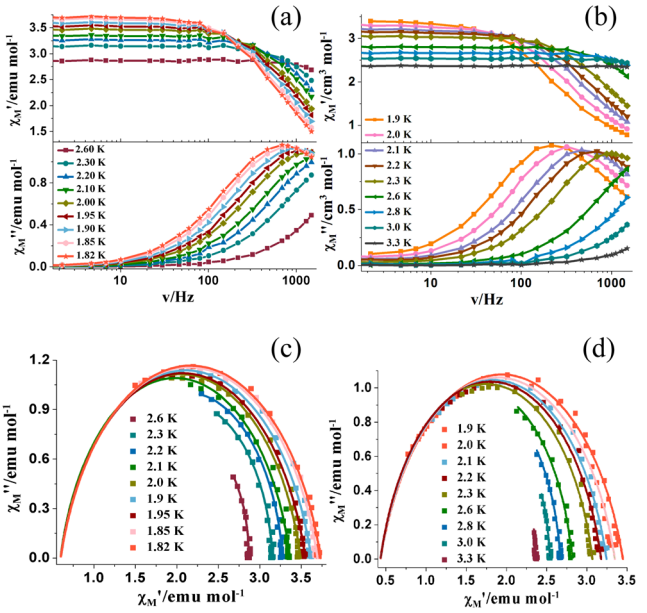

Figure 5. The frequency dependence of χ_M' and χ_M'' signals under zero (a) and 1 kOe (b) dc fields (the solid lines are eye-guided), and the Cole−Cole plots under zero (c) and 1 kOe (d) dc fields for **1**.

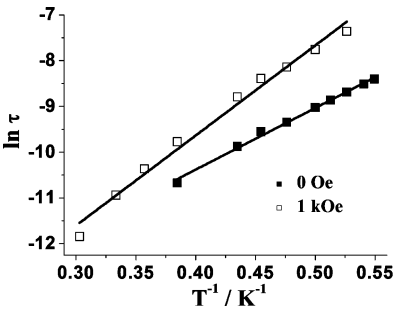

Figure 6. Magnetization relaxation time (τ) versus T^{-1} plots for **1** under zero and 1 kOe dc fields. The solid lines represent the best fits to the Arrhenius law.

The magnetization measurement at 1.8 K reveals that the $M/N\beta$ value at 70 kOe (6.78 $N\beta$ mol^{-1}) is smaller than the expected saturation value of 8.0 $N\beta$ mol^{-1} (Supporting Information, Figure S14). The nonsuperposition of the isofield M versus H/T plots is indicative of the presence of axial zero-field splitting (Supporting Information, Figure S15). A best-fit simulation performed by using Anisoft2.0[37] affords axial and transverse zero-field-splitting parameters of $D = -1.02$ cm^{-1} (−1.47 K) and $E = 0.004$ cm^{-1}, respectively, with $g = 1.92$ and $S_T = 4$. The D value is close to that estimated from the energy barrier (−1.23 K). When the temperature is lowered to 0.5 K, a butterfly-type hysteresis response is observed with no coercivity (Figure 4, inset), possibly due to the relatively fast QTM relaxation process in zero dc field.

In the Ising-like or anisotropic Heisenberg chain models, the correlation length ξ and χT can be related by the following equation: $T = C_{eff} \exp(\Delta_\xi/k_BT)$, where C_{eff} is the effective Curie constant and Δ_ξ is the energy required to create a domain wall along the chain.[2a,38] Thus, a linear dependence of the ln($\chi' T$) versus $1/T$ plot, where χ' is the in-phase ac susceptibility measured at 1 Hz under zero dc field, would prove the magnetic one-dimensional (1D) nature and the presence of significant magnetic anisotropy. For compound **1**, the ln($\chi' T$)

dx.doi.org/10.1021/ic403042p | Inorg. Chem. 2014, 53, 3117−3125

versus $1/T$ plot between 1.8 and 10 K shows a monotonous decreasing of $\ln(\chi'T)$ upon cooling with a negative slope of Δ_ξ (Supporting Information, Figure S16), supporting the SMM nature of **1**.[8,9,39]

It is worth noting that the precursor $[Mn(salen)(H_2O)]_2(ClO_4)_2$ does not show SMM behavior. The switch-on of the SMM behavior of $Mn_2(salen)_2$ dimers was achieved only in a few other systems through Coulombic aggregations[40a,b] or covalent linkages.[40c]

Magnetic Properties of 2. For compound **2**, the magnetic susceptibility above 100 K obeys the Curie–Weiss law with C = 6.43 $cm^3 \cdot K \cdot mol^{-1}$ and θ = −3.95 K (Supporting Information, Figure S17), suggesting a dominant AF interaction in **2**. Upon cooling from 300 K, the $\chi_M T$ value decreases gradually with decreasing temperature and reaches 4.14 $cm^3 \cdot K \cdot mol^{-1}$ at 8.00 K, below which the $\chi_M T$ exhibits a sudden increase to a maximum of 11.01 $cm^3 \cdot K \cdot mol^{-1}$ at 2.50 K and then decreases again (Figure 4). Such a behavior can be attributed to the spin-canting of the antiferromagnetically coupled magnetic centers.

Noting that the $Mn^{III}–O_{ax}$ distances [2.501(4), 2.747(4) Å] and $Mn^{III}–O–Mn^{III}$ angles [97.5(1), 98.2(1)°] in **2** are typical for ferromagnetic coupling in the $Mn_2(SB)_2^{2+}$ dimers,[8] the dominant antiferromagnetic interaction could arise from the O–P–O pathway. This is reasonable considering that the Mn1–O···O–Mn2 torsion angle over the O–P–O bridge is 1.9° in **2**, which is remarkably smaller than that in **1** (96.6°). Thus a relatively strong antiferromagnetic interaction is anticipated to mediate between the Mn^{III} centers over the O–P–O bridges ($2J_2$) in **2**.[23] By employing the Heisenberg dimer model based on the Hamiltonian $H = -2J_2 S_{Mn1} S_{Mn2} + g_{Mn}\beta(S_{Mn1} + S_{Mn2}) \cdot H$ and considering the interdimer interaction (zJ') in the mean field approximation,[27] the magnetic susceptibility data above 14 K can be fit leading to parameters g = 2.07, J_2 = −0.67 K, zJ' = 0.20 K, and $R = 4.26 \times 10^{-3}$ for **2**. The fitting using the alternating chain model with Rojo formula[31] for the magnetic susceptibility data above 14 K leads to parameters g = 2.07, J_1 = 0.20 K, J_2 = −1.71 K, and $R = 1.33 \times 10^{-3}$ for **2**. The negative J_2 value is comparable to those found in the other O–P–O bridged systems.[41] The non-superposition of the isofield M versus H/T plots at low temperatures suggests the presence of axial anisotropy in this compound (Supporting Information, Figure S18).

The linear dependence of the $\ln(\chi'T)$ versus $1/T$ plot, shown in Figure 7a (inset), confirms the 1D nature and the presence of significant magnetic anisotropy in compound **2**. The data in the temperature range of 3.5–7 K can be fit linearly with a positive slope (Δ_ξ) of 6.2 K, which corresponds to the correlation energy. The maximum value of $\ln(\chi'T)$ appears at 2.95 K, below which the $\ln(\chi'T)$ value decreases almost linearly, suggesting the presence of weak antiferromagnetic interactions between the chains.[42]

The dc susceptibility measurements were also performed under different external dc fields in the temperature range of 1.8–20 K. As shown in the inset of Supporting Information, Figure S19, a sharp peak appears in the χ_M versus T plot at ca. 3.00 K under 100 Oe, suggesting an AF ground state. With the increase of the external field, the peak moves to a lower temperature of 2.75 K under 500 Oe, and then disappears above 600 Oe. The strong field dependence of the susceptibility suggests a metamagnetic behavior.

The isothermal magnetization measured at 1.8 K reveals that compound **2** experiences a phase transition from antiferromagnet to weak ferromagnet with the critical field of ca. 500 Oe

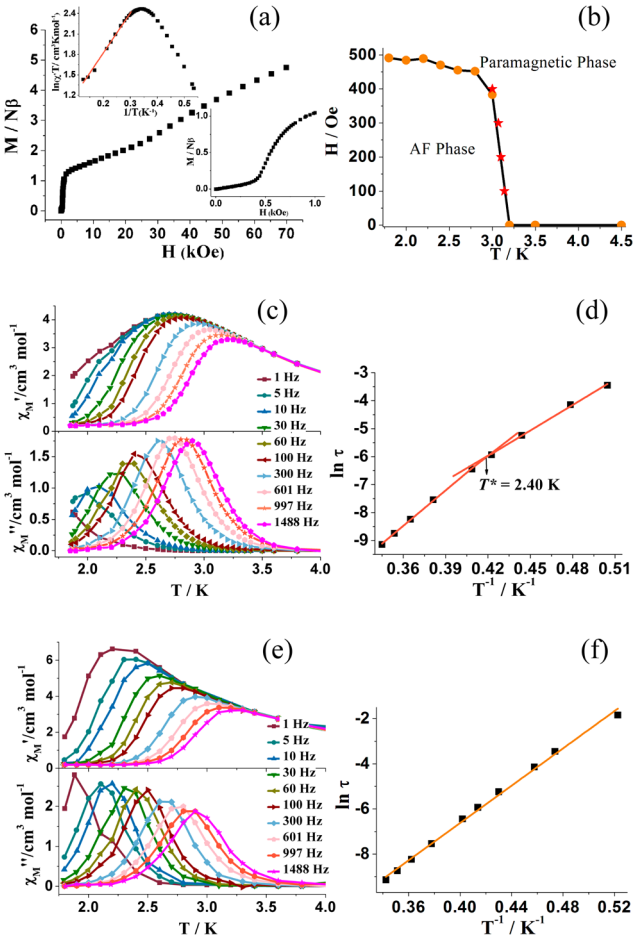

Figure 7. (a) Plots of the M vs H and $\ln(\chi'T)$ vs $1/T$ (inset) for **2**. (b) Magnetic (T, H) phase diagram for **2**, constructed from variable-field (orange filled circle) and variable-temperature (red star) magnetic susceptibility data. The solid line is a guide for the eye. (c, e) The temperature dependence of χ_M' and χ_M'' ac susceptibility under zero (c) and 600 Oe (e) dc field for **2**. The solid lines are eye-guided. (d, f) Arrhenius plots and best linear fits for **2** under zero (d) and 600 Oe (f) dc fields.

at 1.8 K, determined by the dM/dH versus H curve (Figure 7a, Supporting Information, Figure S20). The magnetic energy for H = 500 Oe is 0.07 K, which roughly estimates the interchain AF interaction. The weak ferromagnetism originates from a spin-canted structure within the chain, in accordance with the structure of compound **2** where the Jahn–Teller (JT) axes of $Mn_2(salen)_2$ dimers are not parallel to each other but form an angle (γ) of 65.7°. The canting angle is 18.6°, estimated by $\sin(\alpha/2) = M_r/M_s$, in which M_r is the remanent magnetization and M_s is the saturation magnetization. The canting angle is smaller than γ because the AF interactions tend to align the spin vectors in antiparallel mode. The magnetization is still far from completion when the external field reaches 70 kOe (4.85 $N\beta$ mol^{-1}).

To further study the magnetic phase transition below 2 kOe, field-dependent magnetization data were collected at different temperatures (1.8–3.5 K). By combining the maxima observed in the dM/dH versus H and χ_M versus T data, an (H, T) phase diagram can be constructed, as shown in Figure 7b. Notably, the phase-transition curve extrapolates to T = 0 K at approximately $H_c(0)$ = 500 Oe and vanishes at T_N = 3.2 K. The phase diagram is typical for an antiferromagnet with a

dx.doi.org/10.1021/ic403042p | Inorg. Chem. 2014, 53, 3117–3125

metamagnetic behavior. The $H_c(T)$ line corresponds to an AF/paramagnetic phase transition that occurs when the magnetic field is applied along the easy direction of the magnetization.[43] The small T_N is consistent with the presence of a very weak interchain AF interaction estimated by the critical field (ca. 0.07 K).

Figure 7c shows the temperature-dependent ac susceptibilities of compound **2**, measured in the frequency range of 1−1488 Hz under zero dc field with 3.5 Oe ac field. Slow relaxation of the magnetization is again observed below 4.0 K. The Mydosh φ value is 0.13, ruling out the spin-glass behavior.[44] The relaxation is thermally activated, following Arrhenius law. The temperature dependence of $\ln(\tau)$ exhibits a crossover at 2.4 K, possibly due to the finite-size effect in **2**. Fitting the data of **2** above and below 2.4 K, the Δ/k_B and τ_0 values are 42.3 K and 5.0×10^{-11} s and 30.5 K and 7.0×10^{-9} s, respectively (Figure 7d). The τ_0 values are at least 1 order of magnitude smaller than those for compound **1** but fall in the range for typical SCMs.[2c] The α values simulated from Cole−Cole diagrams at 2.0, 2.5, and 3.0 K are 0.13, 0.08, and 0.04 for **2** (Supporting Information, Figure S22), revealing that the slow relaxation processes have a narrow distribution.

The ac magnetic susceptibility measurements were also performed above the critical field at H_{dc} = 600 Oe with H_{ac} = 3.5 Oe. The frequency dependence of both the χ_M' and χ_M'' signals is observed below ca. 4.0 K. The reversal energy and pre-exponential factor are Δ/k_B = 41.4 K and $\tau_0 = 8.6 \times 10^{-11}$ s, respectively, indicating an SCM behavior (Figure 7e,f). The energy barrier is slightly smaller than that obtained at zero dc field (42.3 K), the reason for which is still not clear to us.

Although compound **2** has an AF ground state, the field-dependent magnetization was measured to 0.5 K. As shown in Figure 4 (inset), the M versus H curve at 0.5 K shows hysteresis with a remnant magnetization (M_r) of 1.20 $N\beta$ mol^{-1} and a large coercivity (H_c) of 11 kOe. The steps observed in the magnetization curve around zero field could be due to the QTM effect. When the temperature is increased to 1.0 K, the M_r and H_c values become ca. 1.32 $N\beta$ mol^{-1} and 3 kOe, respectively. The hysteresis loop disappears at 1.5 K (Supporting Information, Figure S23). Apparently, the magnetization of SCMs can be blocked at very low temperature after it is "magnetized" by an external field. The enhanced magnetic hardness was also observed in a few other systems containing SCM components.[45,46]

CONCLUSIONS

We report the first examples of O−P−O bridged chain compounds embedding $Mn_2(SB)_2$ dimers, namely, $[Mn_2(salen)_2(2\text{-}FC_6H_4PO_3H)](ClO_4)\cdot 1/2CH_3OH$ (**1**) and $[Mn_2(salen)_2(4\text{-}FC_6H_4PO_3H)](ClO_4)$ (**2**). The positional isomerism of the phosphonate ligands leads to a slight difference in the chain structures but completely different magnetic behaviors, for example, an SMM behavior in **1** and the coexistence of SCM and metamagnetism in **2**. The results demonstrate that the magnetic dynamics of paramagnetic chains can be modulated by using structural isomeric bridging ligands. Further work is in progress to explore new SCMs based on phosphonate-bridged $Mn_2(SB)_2$ chain compounds showing higher energy barriers and multifunctions.

ASSOCIATED CONTENT

Supporting Information

Structural data, PXRD, TG, and additional magnetic data. This material is available free of charge via the Internet at http://pubs.acs.org.

AUTHOR INFORMATION

Corresponding Author

*E-mail: lmzheng@nju.edu.cn. Fax: (+86) 25-83314502.

Notes

The authors declare no competing financial interest.

ACKNOWLEDGMENTS

This Work is supported by the National Basic Research Program of China (2010CB923402, 2013CB922102) and the NSF of Jiangsu Province of China (Nos. BK2009009, BK20130054). T.T.W. appreciates Prof. Wei-Xiong Zhang for valuable discussions.

REFERENCES

(1) (a) Glauber, R. J. *J. Math. Phys.* **1963**, *4*, 294−307. (b) Caneschi, A.; Gatteschi, D.; Lalioti, N.; Sangregorio, C.; Sessoli, R.; Venturi, G.; Vindigni, A.; Rettori, A.; Pini, M. G.; Novak, M. A. *Angew. Chem., Int. Ed.* **2001**, *40*, 1760−1763.

(2) (a) Coulon, C.; Miyasaka, H.; Clérac, R. *Struct. Bonding (Berlin, Ger.)* **2006**, *122*, 163−206. (b) Bogani, L.; Vindigni, A.; Sessoli, R.; Gatteschi, D. *J. Mater. Chem.* **2008**, *18*, 4750−4758. (c) Sun, H.-L.; Wang, Z.-M.; Gao, S. *Coord. Chem. Rev.* **2010**, *254*, 1081−1100. (d) Miyasaka, H.; Julve, M.; Yamashita, M.; Clérac, R. *Inorg.Chem.* **2009**, *48*, 3420−3437.

(3) (a) Harris, T. D.; Bennett, M. V.; Clérac, R.; Long, J. R. *J. Am. Chem. Soc.* **2010**, *132*, 3980−3988. (b) Venkatakrishnan, T. S.; Sahoo, S.; Bréfuel, N.; Duhayon, C.; Paulsen, C.; Barra, A.-L.; Ramasesha, S.; Sutter, J.-P. *J. Am. Chem. Soc.* **2010**, *132*, 6047−6056. (c) Liu, T.; Zhang, Y.-J.; Kanegawa, S.; Sato, O. *J. Am. Chem. Soc.* **2010**, *132*, 8250−8251. (d) Dong, D.-P.; Liu, T.; Kanegawa, S.; Kang, S.; Sato, O.; He, C.; Duan, C.-Y. *Angew. Chem., Int. Ed.* **2012**, *51*, 5119−5123. (e) Ding, M.; Wang, B.-W.; Wang, Z.-M.; Zhang, J.-L.; Fuhr, O.; Fenske, D.; Gao, S. *Chem.—Eur. J.* **2012**, *18*, 915−924. (f) Hoshino, N.; Iijima, F.; Newton, G. N.; Yoshida, N.; Shiga, T.; Nojiri, H.; Nakao, A.; Kumai, R.; Murakami, Y.; Oshio, H. *Nat. Chem.* **2012**, *4*, 921−926.

(4) Coulon, C.; Clérac, R.; Wernsdorfer, W.; Colin, T.; Miyasaka, H. *Phys. Rev. Lett.* **2009**, *102*, 167204/1−167204/4.

(5) (a) Toma, L. M.; Lescouëzec, R.; Lloret, F.; Julve, M.; Vaissermann, J.; Verdaguer, M. *Chem. Commun.* **2003**, 1850−1852. (b) Toma, L. M.; Delgado, F. S.; Ruiz-Pérez, C.; Carrasco, R.; Cano, J.; Lloret, F.; Julve, M. *Dalton Trans.* **2004**, 2836−2846. (c) Toma, L. M.; Lescouëzec, R.; Uriel, S.; Llusar, R.; Ruiz-Pérez, C.; Vaissermann, J.; Lloret, F.; Julve, M. *Dalton Trans.* **2007**, 3690−3698. (d) Zheng, Y.-Z.; Xue, W.; Tong, M.-L.; Chen, X.-M.; Grandjean, F.; Long, G. J. *Inorg. Chem.* **2008**, *47*, 4077−4087. (e) Wöhlert, S.; Boeckmann, J.; Wriedt, M.; Näther, C. *Angew. Chem., Int. Ed.* **2011**, *50*, 6920−6923. (f) Toma, L. M.; Ruiz-Pérez, C.; Pasán, J.; Wernsdorfer, W.; Lloret, F.; Julve, M. *J. Am. Chem. Soc.* **2012**, *134*, 15265−15268.

(6) (a) Yoon, J. H.; Ryu, D. W.; Kim, H. C.; Yoon, S. W.; Suh, B. J.; Hong, C. S. *Chem.—Eur. J.* **2009**, *15*, 3661−3665. (b) Yoon, J. H.; Lee, J. W.; Ryu, D. W.; Yoon, S. W.; Suh, B. J.; Kim, H. C.; Hong, C. S. *Chem.—Eur. J.* **2011**, *17*, 3028−3034. (c) Miyasaka, H.; Takayama, K.; Saitoh, A.; Furukawa, S.; Yamashita, M.; Clérac, R. *Chem.—Eur. J.* **2010**, *16*, 3656−3662. (d) Zhang, X.-M.; Wang, Y.-Q.; Wang, K.; Gao, E.-Q.; Liu, C.-M. *Chem. Commun.* **2011**, *47*, 1815−1817. (e) Zhang, S.-Y.; Shi, W.; Lan, Y.; Xu, N.; Zhao, X.-Q.; Powell, A. K.; Zhao, B.; Cheng, P.; Liao, D.-Z.; Yan, S.-P. *Chem. Commun.* **2011**, *47*, 2859−2861.

(7) (a) Roubeau, O.; Clérac, R. *Eur. J. Inorg. Chem.* **2008**, 4325−4342. (b) Jeon, I.-R.; Clérac, R. *Dalton Trans.* **2012**, *41*, 9569−9586. (c) Miyasaka, H.; Yamashita, M. *Dalton Trans.* **2007**, 399−406.
(8) (a) Miyasaka, H.; Clérac, R.; Wernsdorfer, W.; Lecren, L.; Bonhomme, C.; Sugiura, K.-i.; Yamashita, M. *Angew. Chem., Int. Ed.* **2004**, *43*, 2801−2805. (b) Lu, Z. L.; Yuan, M.; Pan, F.; Gao, S.; Zhang, D. Q.; Zhu, D. B. *Inorg. Chem.* **2006**, *45*, 3538−3548. (c) Sawada, Y.; Kosaka, W.; Hayashi, Y.; Miyasaka, H. *Inorg. Chem.* **2012**, *51*, 4824−4832.
(9) Wernsdorfer, W.; Aliaga-Alcalde, N.; Hendrickson, D. N.; Christou, G. *Nature* **2002**, *416*, 406−409.
(10) Saitoh, A.; Miyasaka, H.; Yamashita, M.; Clérac, R. *J. Mater. Chem.* **2007**, *17*, 2002−2012.
(11) (a) Clérac, R.; Miyasaka, H.; Yamashita, M.; Coulon, C. *J. Am. Chem. Soc.* **2002**, *124*, 12837−12844. (b) Miyasaka, H.; Clérac, R.; Mizushima, K.; Sugiura, K.-i.; Yamashita, M.; Wernsdorfer, W.; Coulon, C. *Inorg. Chem.* **2003**, *42*, 8203−8213. (c) Wernsdorfer, W.; Clérac, R.; Coulon, C.; Lecren, L.; Miyasaka, H. *Phys. Rev. Lett.* **2005**, *95*, 237203/1−237203/4. (d) Miyasaka, H.; Saitoh, A.; Yamashita, M.; Clérac, R. *Dalton Trans.* **2008**, 2422−2427. (e) Miyasaka, H.; Julve, M.; Yamashita, M.; Clérac, R. *Inorg. Chem.* **2009**, *48*, 3420−3437.
(12) (a) Ferbinteanu, M.; Miyasaka, H.; Wernsdorfer, W.; Nakata, K.; Sugiura, K.; Yamashita, M.; Coulon, C.; Clerac, R. *J. Am. Chem. Soc.* **2005**, *127*, 3090−3099. (b) Miyasaka, H.; Madanbashi, T.; Saitoh, A.; Motokawa, N.; Ishikawa, R.; Yamashita, M.; Bahr, S.; Wernsdorfer, W.; Clérac, R. *Chem.—Eur. J.* **2012**, *18*, 3942−3954.
(13) Bhowmick, I.; Hillard, E. A.; Dechambenoit, P.; Coulon, C.; Harris, T. D.; Clérac, R. *Chem. Commun.* **2012**, *48*, 9717−9719.
(14) Zhang, W.-X.; Shiga, T.; Miyasaka, H.; Yamashita, M. *J. Am. Chem. Soc.* **2012**, *134*, 6908−6911.
(15) (a) Bai, Y.-L.; Tao, J.; Wernsdorfer, W.; Sato, O.; Huang, R.-B.; Zheng, L.-S. *J. Am. Chem. Soc.* **2006**, *128*, 16428−16429. (b) Xu, H.-B.; Wang, B.-W.; Pan, F.; Wang, Z.-M.; Gao, S. *Angew. Chem., Int. Ed.* **2007**, *46*, 7388−7392. (c) Liu, C.-M.; Zhang, D.-Q.; Zhu, D.-B. *Inorg. Chem.* **2009**, *48*, 4980−4987. (d) Song, X.; Yang, P.; Mei, X.; Li, L.; Liao, D. *Eur. J. Inorg. Chem.* **2010**, 1689−1695. (e) Bai, Y.-L.; Bao, X.; Zhu, S.; Fang, J.; Tao, J. *Dalton Trans.* **2013**, *42*, 1033−1038.
(16) Lecren, L.; Roubeau, O.; Coulon, C.; Li, Y. G.; Le Goff, X. F.; Wernsdorfer, W.; Miyasaka, H.; Clérac, R. *J. Am. Chem. Soc.* **2005**, *127*, 17353−17363.
(17) (a) Chakov, N. E.; Wernsdorfer, W.; Abboud, K. A.; Christou, G. *Inorg. Chem.* **2004**, *43*, 5919−5930. (b) Brockman, J. T.; Stamatatos, T. C.; Wernsdorfer, W.; Abboud, K. A.; Christou, G. *Inorg. Chem.* **2007**, *46*, 9160−9171. (c) Feng, P. L.; Hendrickson, D. N. *Inorg. Chem.* **2010**, *49*, 6393−6395. (d) Yang, C.-I.; Hung, S.-P.; Lee, G.-H.; Nakano, M.; Tsai, H.-L. *Inorg. Chem.* **2010**, *49*, 7617−7619. (e) Yang, C.-I.; Tsai, Y.-J.; Huang, S.-P.; Tsai, H.-L.; Nakano, M. *Chem. Commun.* **2010**, *46*, 5716−5718.
(18) (a) Clearfield, A.; Demadis, K. D. *Metal Phosphonate Chemistry: from Synthesis to Applications;* RSC Publishing: London, 2012. (b) Zheng, L.-M.; Song, H.-H.; Xin, X.-Q. *Comments Inorg. Chem.* **2000**, *22*, 129−149.
(19) Maheswaran, S.; Chastanet, G.; Teat, S. J.; Mallah, T.; Sessoli, R.; Wernsdorfer, W.; Winpenny, R. E. P. *Angew.Chem., Int. Ed.* **2005**, *44*, 5044−5048.
(20) (a) Sun, Z.-M.; Prosvirin, A. V.; Zhao, H.-H.; Mao, J.-G.; Dunbar, K. R. *J. Appl. Phys.* **2005**, *97*, 10B305/1−10B305/3. (b) Palii, A. V.; Reu, O. S.; Ostrovsky, S. M.; Klokishner, S. I.; Tsukerblat, B. S.; Sun, Z.-M.; Mao, J.-G.; Prosvirin, A. V.; Zhao, H.-H.; Dunbar, K. R. *J. Am. Chem. Soc.* **2008**, *130*, 14729−14738.
(21) (a) Bellitto, C.; Bauer, E. M.; Righini, G. *Inorg. Chim. Acta* **2008**, *361*, 3785−3799. (b) Huang, J.; Bao, S.-S.; Ling, L.-S.; Zhu, H.; Li, Y.-Z.; Pi, L.; Zheng, L.-M. *Chem.—Eur. J.* **2012**, *18*, 10839−10842. (c) Guo, L.-R.; Bao, S.-S.; Liu, B.; Zeng, D.; Zhao, J.; Du, J.; Zheng, L.-M. *Chem.—Eur. J.* **2012**, *18*, 9534−9542. (d) Li, J.-T.; Keene, T. D.; Cao, D.-K.; Decurtins, S.; Zheng, L.-M. *CrystEngComm* **2009**, *11*, 1255−1260.
(22) (a) Bao, S.-S.; Liao, Y.; Su, Y.-H.; Liang, X.; Hu, F.-C.; Sun, Z.; Zheng, L.-M.; Wei, S.-Q.; Alberto, R.; Li, Y.-Z.; Ma, J. *Angew. Chem., Int. Ed.* **2011**, *50*, 5504−5508. (b) Yang, T.-H.; Liao, Y.; Zheng, L.-M.; Dinnebier, R. E.; Su, Y.-H.; Ma, J. *Chem. Commun.* **2009**, 3023−3025. (e) Cai, Z.-S.; Bao, S.-S.; Zheng, L.-M. *Acta Chim. Sin. (Engl. Ed.)* **2013**, *71*, 555−559. (f) Ren, M.; Bao, S.-S.; Hoshino, N.; Akutagawa, T.; Wang, B.; Ding, Y.-C.; Wei, S.; Zheng, L.-M. *Chem.—Eur. J.* **2013**, *19*, 9619−9628.
(23) Huang, J.; Liu, P.-Y.; Zhu, H.; Bao, S.-S.; Zheng, L.-M.; Ma, J. *ChemPlusChem* **2012**, *77*, 1087−1095.
(24) Bernot, K.; Luzon, J.; Sessoli, R.; Vindigni, A.; Thion, J.; Richeter, S.; Leclercq, D.; Larionova, J.; van der Lee, A. *J. Am. Chem. Soc.* **2008**, *130*, 1619−1627.
(25) (a) Przychodzeń, P.; Lewiński, K.; Bałanda, M.; Pełka, R.; Rams, M.; Wasiutyński, T.; Guyard-Duhayon, C.; Sieklucka, B. *Inorg. Chem.* **2004**, *43*, 2967−2974. (b) Shyu, H.-L.; Wei, H.-H.; Wang, Y. *Inorg. Chim. Acta* **1999**, *290*, 8−13.
(26) Bennett, J. A.; Hope, E. G.; Singh, K.; Stuart, A. M. *J. Fluorine Chem.* **2009**, *130*, 615−620.
(27) Kahn. O. *Molecular Magnetism;* VCH: New York, 1993.
(28) *SAINT-Plus,* version 6.02; Bruker Analytical X-ray System: Madison, WI, 1999.
(29) Sheldrick, G. M. *SHELXTL-97;* Universität of Göttingen: Göttingen, Germany, 1997.
(30) (a) Thalladi, V. R.; Weiss, H.-C.; Bläser, D.; Boese, R.; Nangia, A.; Desiraju, G. R. *J. Am. Chem. Soc.* **1998**, *120*, 8702−8710. (b) Takahashi, O.; Kohno, Y.; Nishio, M. *Chem. Rev.* **2010**, *110*, 6049−6076.
(31) Cortes, R.; Drillon, M.; Solans, X.; Lezama, L.; Rojo, T. *Inorg. Chem.* **1997**, *36*, 677−683.
(32) (a) Miyasaka, H.; Saitoh, A.; Abe, S. *Coord. Chem. Rev.* **2007**, *251*, 2622−2664. (b) Wang, T.-T.; Ren, M.; Bao, S.-S.; Zheng, L.-M. *Eur. J. Inorg. Chem.* **2014**, 1042−1050.
(33) Thomas, L.; Lionti, F.; Ballou, R.; Gatteschi, D.; Sessoli, R.; Barbara, B. *Nature* **1996**, *383*, 145−147.
(34) Cole, K. S.; Cole, R. H. *J. Chem. Soc.* **1941**, *9*, 341−351.
(35) Gatteschi, D.; Sessoli, R.; Villain, J. *Molecular Nanomagnets;* Oxford University Press: Oxford, U.K., 2006.
(36) (a) Sessoli, R.; Gatteschi, D.; Caneschi, A.; Novak, M. A. *Nature* **1993**, *365*, 141−143. (b) Sessoli, R.; Tsai, H. L.; Schake, A. R.; Wang, S.; Vincent, J. B.; Folting, K.; Gatteschi, D.; Christou, G.; Hendrickson, D. N. *J. Am. Chem. Soc.* **1993**, *115*, 1804−1816. (c) Aromi, G.; Brechin, E. K. *Struct. Bonding (Berlin)* **2006**, *122*, 1−69.
(37) Shores, M. P.; Sokol, J. J.; Long, J. R. *J. Am. Chem. Soc.* **2002**, *124*, 2279−2292.
(38) (a) Loveluck, J. M.; Lovesey, S. W.; Aubry, S. *J. Phys. C: Solid State Phys.* **1975**, *8*, 3841−3856. (b) Nakamura, K.; Sasada, T. *J. Phys. C: Solid State Phys.* **1978**, *11*, 331−343.
(39) Lecren, L.; Wernsdorfer, W.; Li, Y.-G.; Vindigni, A.; Miyasaka, H.; Clérac, R. *J. Am. Chem. Soc.* **2007**, *129*, 5045−5051.
(40) (a) Wu, Q.; Li, Y.-G.; Wang, Y.-H.; Clerac, R.; Lu, Y.; Wang, E.-B. *Chem. Commun.* **2009**, 5743−5745. (b) Sawada, Y.; Kosaka, W.; Hayashi, Y.; Miyasaka, H. *Inorg. Chem.* **2012**, *51*, 4824−4832. (c) Wang, T.-T.; Bao, S.-S.; Ren, M.; Cai, Z.-S.; Zheng, Z.-H.; Xu, Z.-L.; Zheng, L.-M. *Chem.—Asian J.* **2013**, *8*, 1772−1775.
(41) (a) Cao, D.-K.; Xiao, J.; Li, Y.-Z.; Clemente-Juan, J. M.; Coronado, E.; Zheng, L.-M. *Eur. J. Inorg. Chem.* **2006**, 1830−1837. (b) Youngme, S.; Phuengphai, P.; Pakawatchai, C.; van Al-bada, G. A.; Reedijk, J. *Inorg. Chim. Acta* **2005**, *358*, 2125−2128. (c) Song, H.-H.; Yin, P.; Zheng, L.-M.; Korp, J. D.; Jacobson, A. J.; Gao, S.; Xin, X.-Q. *J. Chem. Soc., Dalton Trans.* **2002**, 2752−2759.
(42) Coulon, C.; Clérac, R.; Lecren, L.; Wernsdorfer, W.; Miyasaka, H. *Phys. Rev. B: Condens. Matter Mater. Phys.* **2004**, *69*, 132408/1−132408/4.
(43) Harris, T. D.; Coulon, C.; Clérac, R.; Long, J. R. *J. Am. Chem. Soc.* **2011**, *133*, 123−130.
(44) Mydosh, J. A. *Spin Glasses: An Experimental Introduction;* Taylor & Francis: London, 1993.

(45) (a) Ishii, N.; Okamura, Y.; Chiba, S.; Nogami, T.; Ishida, T. *J. Am. Chem. Soc.* **2008**, *130*, 24−25. (b) Ishida, T.; Okamura, Y.; Watanabe, I. *Inorg. Chem.* **2009**, *48*, 7012−7014. (c) Sessoli, R. *Angew. Chem., Int. Ed.* **2008**, *47*, 5508−5510.
(46) Wang, P.-F.; Duan, Y.; Clemente-Juan, J. M.; Song, Y.; Qian, K.; Gao, S.; Zheng, L.-M. *Chem.—Eur. J.* **2011**, *17*, 3579−3583.